Biophysical Chemistry, 43 (1992) 117–137
Elsevier Science Publishers B.V., Amsterdam

BIOCHE 01656

Reaction rate enhancement by surface diffusion of adsorbates

Dong Wang [a], Shi-Yuan Gou [b] and Daniel Axelrod [a,c]

[a] *Biophysics Research Division,* [b] *Department of Mechanical Engineering, and* [c] *Department of Physics, University of Michigan, Ann Arbor, MI 48109 (USA)*

(Received 13 August 1991; accepted in revised form 11 February 1992)

Abstract

Ligands can be captured by a surface target through either direct bulk diffusion or surface diffusion following reversible adsorption to the surface. We have solved a steady state boundary value problem for a perfect sink disk target in the surface, taking into account bulk and surface diffusion coefficients D and D_s and adsorption/desorption kinetic rate constants k_a and k_d at non-target regions. Solutions have been successfully found by numerical computation. The results show that the rate of capture from the surface depends non-linearly on D_s, D, k_a, k_d and geometrical dimensions. In particular, we demonstrate that not only is the non-target region equilibrium constant K_{eq} $(= k_a/k_d)$ important in determining the rate of capture from the surface, but so are the kinetic rate constants k_a and k_d separately. In all cases, the surface adsorption/diffusion combination enhances the total rate of capture. The results should be useful for predicting reaction rates of biological membrane bound receptor clusters and substrate-immobilized enzymes.

Keywords: Surface diffusion; Membrane receptors; Reaction kinetics; Surface adsorption; Mathematical model; Reduction of dimensionality

1. Introduction

Surfaces are involved in many chemical and biological reactions. A surface often has a direct effect on the kinetics and mechanism of the reaction, particularly if one reactant (called the "target" here) is confined to the surface and the other (called the "ligand" here) is dissolved in the bulk. There are two distinct diffusive pathways for the bulk-dissolved ligand to be captured by the target sink (see Fig. 1): by pure three-dimensional (3D) diffusion to the "specific" target; or by 3D diffusion to a "non-specific" (i.e., non-target) region of the surface followed by adsorption and two-dimensional (2D) surface diffusion to the target. A more general intermediate case can occur if the adsorption to the surface is reversible. In principle, the rates of capture from 3D and from 2D affect each other, and the sum of the two rates in steady state is always greater than the steady state rate of capture that would have occurred with a non-adsorbing surface.

Adam and Delbrück [1] first introduced the idea of reaction rate enhancement by "reduction of dimensionality" and suggested certain biologi-

Correspondence to: Dr. Daniel Axelrod, Biophysics Research Division, University of Michigan, 2200 Bonisteel Blvd., Ann Arbor, MI 48109. Tel. # 313-764-5280.

cal systems where it might be operant (e.g., pheromones and olfactory organs in insects). Other possibilities are reviewed by Axelrod [2]. Berg and Purcell [3] did a quantitative study of the 3D/2D reduction of dimensionality problem for a surface containing discrete perfect sink targets in steady state. They derived a criterion by which the 2D rate of capture (i.e., capture from the surface via 2D diffusion) might become important, provided that the target surface concentration is low enough so that the total rate of capture (i.e., capture from both 2D and 3D) is much less than its maximum possible value (defined for a hypothetical cell whose entire surface is a perfect sink). Their criterion asserts that the 2D rate of capture is proportional only to the equilibrium constant for adsorption to non-target areas K_{eq} $(=k_a/k_d)$ and to the surface diffusion coefficient D_s, and that it is independent of the bulk diffusion coefficient D or the kinetic rate constants k_a, k_d for non-specific adsorption/desorption. According to their theory, the 2D rate of capture per target decreases as the surface target concentration decreases. More recently, Otto Berg [4] analytically solved a mathematical model of reversible adsorption and surface diffusion to a single 2D perfect sink target. However, as Berg mentions, that model is most appropriate for the limit where the kinetic adsorption and desorption rate constants approach infinity.

Cukier [5] has presented an elegant approximate mathematical formalism for a somewhat different but related problem, in which the target is a perfect sink circular ring instead of a disk, the adsorption/desorption process is assumed to be saturable and can occur anywhere on the surface (even directly into the central area of the ring), and the bulk concentration is assumed to be constant everywhere. This formalism would be expected to correspond best to the above models where the targets are small compared to the whole surface.

Here, we present a general computational solution of the problem of surface-confined perfect sinks able to receive ligands from either 2D or 3D. Solutions are found by numerical calculations on a personal computer. Our results show that the 2D rate of capture per target not only is a function of K_{eq}, but also depends on the adsorption/desorption kinetic rate constants k_a and k_d separately. In addition, this 2D rate of capture has a non-linear dependence on D_s and it depends upon the value of the 3D bulk diffusion coefficient. Also, the 2D rate of capture per target increases (rather than decreases as in the Berg and Purcell model) and approaches an asymptote as the surface target concentration decreases. These significant discrepancies between our results and those of Berg and Purcell evidently arise from their more restrictive assump-

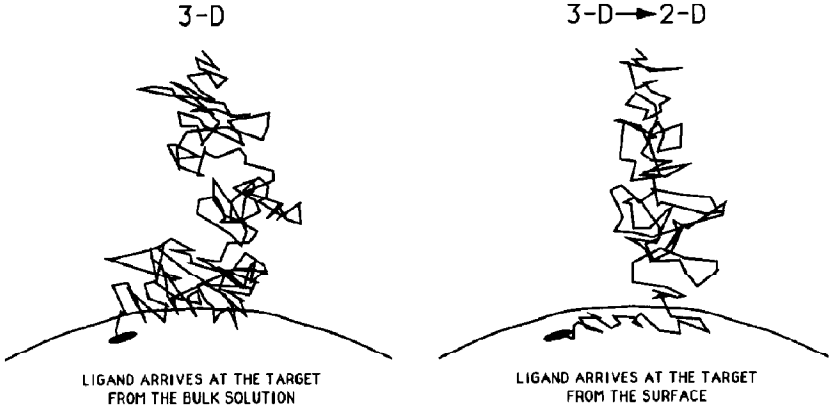

Fig. 1. Two possible pathways for the capture of ligands by the target.

tions. It will also be shown that our results agree with those from Otto Berg, but only in the limit when k_a and $k_d \to \infty$.

All of the above models assume that the target is a perfect sink. Several processes in industrial chemistry and cell biology can conceivably be described by a model of 3D/2D diffusion to a perfect sink. For example, in industrial applications, enzymes immobilized on the surfaces of artificial matrices are used to catalyze the conversion of large quantities of bulk dissolved ligands into useful products [6]. If the rate of conversion of a particular ligand to product is limited only by the time necessary for that ligand to diffuse to an enzyme, then that enzyme can be modeled as a perfect sink for the ligand. Numerous biological cell surface enzymes also can act like immobilized sinks for bulk-dissolved ligands. For example, acetylcholinesterase resides in the basal lamina at the muscle cell surface of a synapse and captures acetylcholine, breaking it into acetate and choline and thereby shortening the time that free acetylcholine is available to interact with the separate acetylcholine receptors. If acetylcholine nonspecifically adsorbs to the cell surface, the breakdown reaction rate will be affected.

Another possible example of a naturally occurring 2D perfect sink is the general class of membrane transporters. A membrane transporter transfers a specific type of molecule (e.g., sugars, amino acids, nucleotides or some cell metabolites) across cell membranes. If we assume that the transporter functions unidirectionally, and that the time required for transferring is much smaller than the time between arrivals of molecules, then the transporter can be modeled as a perfect sink.

A distinctive feature of a perfect sink is that it creates, and is affected by, a local diffusion depletion zone around itself in steady state. However, many cell surface receptors cannot be modeled as perfect sinks. In some situations, receptors reversibly bind ligands, releasing them unaltered back into solution, and thereby establishing an equilibrium with no concentration gradients. Other receptors bind irreversibly but with a capacity of just one ligand, followed by internalization of the whole complex (often by internalization at a coated pit), as new receptors are continuously incorporated into the membrane in a steady state process. If these new replacement receptors are incorporated in a spatially random pattern (only an approximation to biological reality), then the fresh unoccupied receptors see a uniform probability density of ligand in their vicinities, and again, no local depletion zones are relevant for calculating rates. (A relevant global depletion zone still develops near the surface.) However, a pre-existing *cluster* of many receptors (e.g., for neurotransmitters, hormones, and pheromones) still can be modeled as a perfect sink if the cluster as a whole does not readily become saturated by captured ligands. Certain cell surface receptors are found in clusters before capturing ligands, e.g., acetylcholine receptors in both synapses and in aneural muscle cultures, and nerve growth factor receptors [7].

If the concentration of surface targets is sufficiently high [3], then even rapid surface diffusion of nonspecifically adsorbed ligands may not significantly speed up encounters with targets. McCloskey and Poo [8] have presented a review of selected biological data which suggests that some potential membrane targets do indeed present a sufficiently high concentration so that surface diffusion would not be helpful. However, some other biological membranes may have lower surface target concentrations so that the rate of capture of ligands from the surface could be significant. More experimental data is necessary to determine the surface target concentrations of other systems.

Another possible instance of rate enhancement entails the reduction of dimensionality of diffusion from three to one. One example of a system where this type of rate enhancement might occur is the non-specific binding and possible 1D diffusion of a repressor protein along a DNA strand before it encounters its specific operator [9].

The results from this theoretical study can be used for answering questions about the surface contribution to the rate of capture in a real system if the key dynamic parameters—the surface diffusion coefficient and the non-specific reversible adsorption/desorption kinetic rate con-

stants–are known. Fortunately, these parameters often can be calculated from the results of a variety of techniques, notably by total internal reflection/fluorescence recovery after photobleaching (TIR/FRAP) [10–13].

2. Mathematical model

We will refer to the immobile 2D-confined enzymes, transporters, receptor clusters, etc. as *targets*, and the diffusing hormones, agonists, antigens, etc. as *ligands*. Binding (assumed irreversible) between the two classes is referred to as *specific* binding. Binding (assumed reversible) of ligands to all other areas of the surface is referred to as *non-specific* adsorption.

Each target is modeled as a disk sink with radius R_1 embedded in the surface (see Fig. 2). The boundary for each target is chosen to be a cylinder of radius R_2 and height H, with the target at the center of its bottom surface. R_2 is determined by the target concentration on the cell surface. For a cell that has many targets uniformly distributed on its surface, each target on the average occupies an area A_r that is equal to the total area divided by the total number of targets. If A_r is flat, it can be modeled as a circle with the target in the center, R_2 is defined as the radius of that circle.

2.1 Definitions

Notation definitions are summarized here and explained later as necessary.

C is the bulk (3D) concentration of ligands (number/cm^3) and C_s the surface (2D) concentration of ligands (number/cm^2). The non-specific binding reaction is:

$$C \underset{k_d}{\overset{k_a}{\rightleftharpoons}} C_s \tag{1}$$

where k_a is the adsorption rate constant of ligands to non-target areas (cm/s), k_d the desorption rate constant of ligands from non-target areas (s^{-1}), and K_{eq} the equilibrium constant for ligand adsorption to non-target areas (cm) equal to k_a/k_d. The diffusion coefficients are: D the bulk diffusion coefficient of ligands (cm^2/s), and

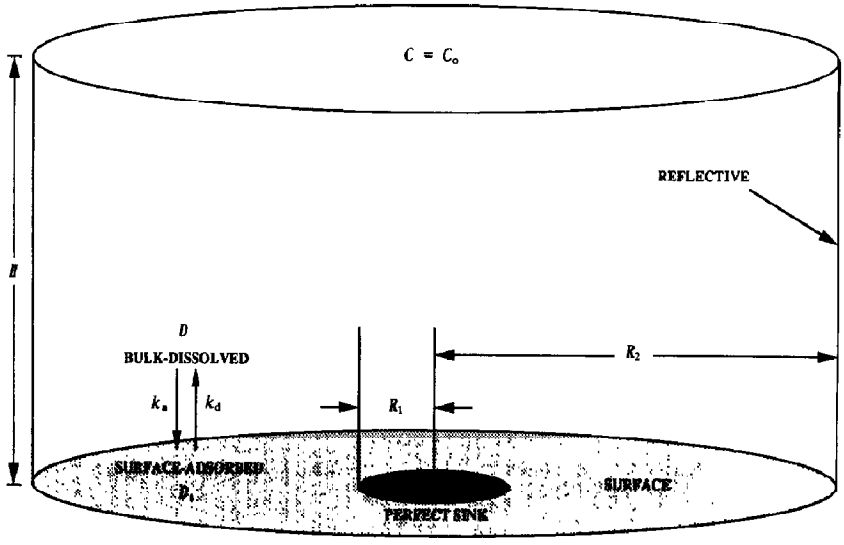

Fig. 2. Geometry and boundary conditions. A disk perfect sink is embedded in the center at the bottom of the cylinder.

D_s the surface diffusion coefficient of ligands in nont-arget areas (cm^2/s). The geometrical features are: R_1 the radius of the target (cm), R_2 the radius of the cylinder (cm), and H the height of the cylinder (cm). The flux rates per target are: F_{2D} the rate of capture of ligands by the target from the (2D) surface (number/s). F_{3D} the rate of capture of ligands by the target from the (3D) bulk (number/s), and F_{tot} the total rate of capture of ligands ($F_{2D} + F_{3D}$) by the target (number/s), respectively. f_{2D} is the fraction of the total rate of capture occurring from the 2D surface, i.e. F_{2D}/F_{tot}. F_{max} is the maximum possible flux assuming $R_1 = R_2$ (number/s), and F_0 is the rate of capture assuming $D_s = 0$ (number/s). In addition, we will refer to one other rate, defined for a limiting geometry, viz. F_0^∞ the rate of capture assuming the boundary is set to infinity and $D_s = 0$. This special case is called Weber's disk, discussed in Crank [14] where it is shown that:

$$F_0^\infty = 4DR_1C_0 \tag{2}$$

2.2 3D diffusion equation in steady state

$$\nabla^2 C(r, z) = 0 \tag{3}$$

2.3 2D diffusion equation in steady state

For non-target regions of the surface $R_1 < r < R_2$, a source term and a sink term on the right represent non-specific adsorption and desorption, respectively, at the surface:

$$D_s \nabla^2 C_s(r) = -k_a C(r, 0) + k_d C_s(r) \tag{4}$$

2.4 Boundary conditions

A finite concentration at a finite height $z = H$ must be maintained for a steady state solution to exist:

$$C(r, H) = C_0 \tag{5}$$

The ligand concentration at the perfect sink target must be zero:

$$C(r \leqslant R_1, 0) = 0 \tag{6}$$

$$C_s(r \leqslant R_1) = 0 \tag{7}$$

The walls of the cylinder are reflective, equivalent to zero net flow across boundaries of target domains:

$$\left.\frac{\partial C(r, z)}{\partial r}\right|_{r=R} = 0 \tag{8}$$

$$\left.\frac{\partial C_s(r)}{\partial r}\right|_{r=R_2} = 0 \tag{9}$$

The bulk concentration gradient in the z-direction near the surface is proportional to the net (adsorption minus desorption) flux of ligand adsorbing at the surface for all $R_1 < r < R_2$:

$$D\left.\frac{\partial C(r, z)}{\partial z}\right|_{z=0} = k_a C(r, 0) - k_d C_s(r) \tag{10}$$

It is this rather complicated boundary condition which necessitates a numerical rather than analytical solution to the problem. If, instead of eq. (10), we had $\partial C(r, z)/\partial z \mid_{z=0} = 0$ for $R_1 < r < R_2$, then the non-target region could be considered to be a perfect reflector. For the purpose of calculating fluxes in such a case, the condition of perfect reflection can be simulated simply by setting $D_s = 0$ in our model, as can be seen by combining eqs. (4) and (10).

Because these boundary conditions all have azimuthal symmetry, C and C_s also have azimuthal symmetry. Hence, C is a function only of r and z, and C_s a function only of r.

2.5 Rates of capture per target

The rates of capture per target region are equal to the integrated diffusive fluxes. A ligand can be captured either through bulk or surface diffusion:

$$F_{3D} = \int_0^{R_1} D\left.\frac{\partial C(r, z)}{\partial z}\right|_{z=0} 2\pi r \, dr \tag{11}$$

$$F_{2D} = D_s \left. \frac{\partial C_s(r)}{\partial r} \right|_{r=R_1} 2\pi R_1 \quad (12)$$

F_{max} is defined by assuming the whole bottom area of the cylinder is a perfect sink. It can easily be found by solving the 3D diffusion equation, and the result is:

$$F_{max} = \pi R_2^2 D C_0 / H \quad (13)$$

2.6 Conversion to dimensionless parameters

These equations can be made dimensionless in order to highlight the independent variables and to facilitate the analysis of the results. We define the following variables and operators:

$$C' \equiv C/C_0 \quad (14)$$

$$C_s' \equiv C_s/(DR_1C_0/D_s) \quad (15)$$

$$r' \equiv r/R_1 \quad (16)$$

$$z' \equiv z/R_1 \quad (17)$$

$$\nabla'^2 \equiv R_1^2 \nabla^2 \quad (18)$$

where the derivatives of ∇'^2 are taken with respect to the primed variables r' and z'.

We also define the following ratios of parameters which serve as independent variables:

$$a_1 \equiv R_2/R_1 \quad (19)$$

$$a_2 \equiv H/R_1 \quad (20)$$

$$a_3 \equiv k_a R_1/D \quad (21)$$

$$a_4 \equiv k_d R_1^2/D_s \quad (22)$$

Equations (3)–(10) can now be rewritten in dimensionless form as follows.

3D diffusion equation:

$$\nabla'^2 C' = 0 \quad (23)$$

2D diffusion equation:

For $1 < r' < a_1$,

$$\nabla'^2 C_s' = -a_3 C' + a_4 C_s' \quad (24)$$

Boundary conditions:

$$C'(a_2) = 1 \quad (25)$$

$$C'(r' \le 1, 0) = 0 \quad (26)$$

$$C_s'(r' \le 1) = 0 \quad (27)$$

$$\left. \frac{\partial C'}{\partial r'} \right|_{r'=a_1} = 0 \quad (28)$$

$$\left. \frac{\partial C_s'}{\partial r'} \right|_{r'=a_1} = 0 \quad (29)$$

For $1 < r' < a_1$,

$$\left. \frac{\partial C'}{\partial z'} \right|_{z'=0} = a_3 C' - a_4 C_s' \quad (30)$$

Rates of capture per target:

$$F_{3D} = DC_0R_1 \int_0^1 \left. \frac{\partial C'}{\partial z'} \right|_{z'=0} 2\pi r' \, dr' \quad (31)$$

$$F_{2D} = DC_0R_1 2\pi \left. \frac{\partial C_s'}{\partial r'} \right|_{r'=1} \quad (32)$$

Although there are eight physical parameters (R_1, R_2, H, D, D_s, k_a, k_d, and C_0), there are only four independent variables (a_1, a_2, a_3, and a_4). This means that for the same set of independent variables but different physical parameters, the solutions for C and C_s each change only by a multiplicative factor (although possibly a different factor for C and C_s). Fraction f_{2D} remains constant, however; it is only a function of the independent variables.

Variables a_1 and a_2 are purely geometrical; they are the radius and height, respectively, of the cylinder normalized with respect to the radius of the sink. All of other physical parameters are incorporated into a_3 and a_4, the normalized adsorption and desorption rate constants, respectively. In particular, changing only k_a and D by the same factor will not change a_3, and thereby will not change the solutions for C' and C_s'. Likewise, changing only k_d and D_s by the same factor will change neither a_4 nor the solutions for C' and C_s'.

3. Previous results

Berg and Purcell [3] studied a similar problem for a plane by a somewhat different approach, denoted here as the "BP model". Under the limit

that $F_{2D} \ll F_{max}$ and $F_{3D} \ll F_{max}$, their results for rates of capture per target are, in our notation:

$$F_{2D}^{BP} = \frac{2\pi D_s K_{eq} C_0}{\ln(4R_2/3R_1)} \quad (33)$$

$$F_{3D}^{BP} = 4DR_1C_0 \quad (34)$$

They therefore concluded that the 2D capture rate will dominate ($F_{2D} > F_{3D}$) if

$$\frac{\pi D_s K_{eq}}{2DR_1} > \ln(4R_2/3R_1) \quad (35)$$

Equation (33) was derived for a planar surface by calculating the distribution of times-to-capture $f(t_c)$ assuming a uniform surface concentration of ligands, and then averaging the times-to-capture t_c over all possible positions. Under this assumption, $f(t_c)$ is exponential:

$$f(t_c) = \frac{1}{\langle t_c \rangle} e^{-t_c/\langle t_c \rangle} \quad (36)$$

and the mean time-to-capture (in our notation) is given by

$$\langle t_c \rangle = \frac{R_2^2}{2D_s}\left[\ln\left(\frac{R_2}{R_1}\right) - \frac{3}{4}\right] \quad (37)$$

Berg and Purcell assume that the reciprocal of $\langle t_c \rangle$ is proportional to the 2D flux rate. This is questionable, particularly considering that the 2D flux rate then approaches zero as R_2 approaches infinity. Moreover, if the target is a perfect sink, the presence of local depletion zones invalidate eqs. (33–37) for the following two reasons:

(a) In deriving eqs. (33), (36), and (37), it was assumed that the bulk concentration was uniform (and set equal to C_0) and that the bulk and the surface are in equilibrium. These assumptions lead to a uniform surface concentration of ligands and to F_{2D}^{BP} (eq. 33) independent of the geometry in the z-direction (i.e., the height of the cylinder). However, a perfect sink target will always generate a ligand depletion zone in both the surface and bulk concentrations near the target. Therefore, those ligands near the target—those with the smallest times-to-capture—should be less weighted during averaging in the calculation of $f(t_c)$. This means that $f(t_c)$ of eq. (36) overestimates the shorter times, and the correct mean time-to-capture $\langle t_c \rangle$ should be greater than that given in eq. (37). The depth, shape, and size of the depletion zone on the surface should depend on the bulk and surface diffusion coefficients and on the surface kinetic rate constants, since these parameters affect the replenishment rate of a surface depletion zone. Thus, both $f(t_c)$ and $\langle t_c \rangle$, and thereby F_{2D}, should depend on D, k_a, and k_d as well as on D_s, R_1, and R_2.

(b) When deriving eq. (34), a sphere was used with small circular sinks sparsely and uniformly distributed on its surface. The surface outside the sinks was assumed to be perfectly reflecting, i.e., the 2D rate of capture is zero. The F_{3D}^{BP} for each sink in the BP model is the same as that the capture rate F_0^{∞} for the case of the Weber's disk (eq. 2), in which a single disk sink is embedded in an infinite reflecting surface with the concentration at infinity held constant. However, when the 2D route does make some contribution to the rate of capture, the surface cannot be considered to be a perfect reflector. In fact, the depletion zone on the surface will inevitably affect the shape and depth of the depletion zone in the bulk and thereby alter the 3D rate of capture.

In view of above two considerations, the criterion for dominance of the 2D rate over the actual 3D rate will be somewhat different in general from eq. (35).

Otto Berg [4] proposed a model (denoted here as the "OB model") similar to the BP model and our model, but with some important differences. In the OB model, the boundary is set at infinity with the concentration held constant. Since only one target sink on the infinite planar surface is modeled, the dependence of the rate of capture on the surface target density can not be analyzed through this model. Also, the target itself is considered to have the same association rate constant from the bulk as does the rest of the surface; i.e., eq. (30) is valid over the whole surface $0 < r' < a_1$, not just $1 < r' < a_1$. As discussed by the author, this extended boundary condition may not be appropriate in general, but as k_a (and also k_d for a constant K_{eq}) approaches infinity, the reversible kinetic behavior of the target itself

should not matter. At this limit, both OB model and ours should agree if the boundary in our model is positioned far out enough. Results from the OB model in our notation are:

$$f_{2D}^{OB} = \frac{2\left(\frac{a_3}{a_4}\right)\int_0^\infty \frac{J_1^2(x)(1+a_3^{-1}x)}{1+(a_3/a_4)x+a_4x^2}\,dx}{1-\int_0^\infty \frac{J_1(x)J_2(x)}{1+(a_3/a_4)x+a_4x^2}\,dx} \quad (38)$$

and

$$F_{tot}^{OB} = \pi D R_1 C_0 \Bigg/ \left[2\int_0^\infty \frac{[J_1(x)/x]^2(1+a_3^{-1}x)}{1+(a_3/a_4)x+a_4x^2}\,dx - f_{2D}^{OB}\int_0^\infty \frac{[J_1(x)/x]J_2(x)(1+a_3^{-1}x)}{1+(a_3/a_4)x+a_4x^2}\,dx \right] \quad (39)$$

4. Computer-generated solution

Finite difference methods [15] were used to numerically solve the boundary value problem for C and C_s posed in eqs. (23)–(30). Since the expected depletion zone is on the order of the size of the sink in the bulk, the area near the sink should be the most heavily sampled to retain accuracy while reducing the computational time. A non-uniform grid derived from a coordinate transformation [16] was employed in order to sample points more densely near the edge of the target on r-coordinate and near the target on the z-coordinate. All calculations were performed on a 486-based 33 Mhz MS-DOS personal computer using MicroSoft FORTRAN 5.0-compiled programs. For each set of parameters, the computer required about 2 to 15 minutes to obtain the solutions.

Solutions for concentrations and fluxes of this boundary value problem are functions of the four independent variables a_i. Plotting the complete results would thereby require a five dimensional graph. Therefore, we present results here based on a rather restricted range of parameters that nonetheless can answer specific questions and be compared with the results of other models. But the programs can be used to find solutions over a wider range of parameters and are available upon request.

4.1 Verification

To verify the validity of our geometry, boundary conditions, and computational procedures, we compare some predictions of our model with those of BP model in cases where both models are applicable. First, there is the question of geometry. Most biological cells are neither spherical nor flat, nor are they bathed in an infinite extent of soluble ligand. Rather, the reservoir of ligand is likely to be a confined space between two cell surfaces that curve while maintaining some separation distance (e.g., pre- and post-synaptic membranes). One of the membranes is often a source of ligand while the other contains the targets. The BP model assumes a ligand bath of infinite extent when calculating F_{3D}; our geometry specifies a finite depth of solution H between the source membrane of ligand and the target membrane. The total capture rate in our model is clearly a function of H for a fixed ligand concentration at $z = H$, but one might expect that the relative contribution of 2D and 3D diffusion would not be a strong function of H. Nevertheless, there is some range of H in a our model for which the absolute rate of 3D capture (in the absence of 2D diffusion) should agree with a spherical model. As discussed previously, the BP model gives $F_{3D}^{BP}/F_0^\infty = 1$ (see eqs. 2 and 34), which is derived assuming that the target area is a very small fraction of the total surface area. In that same range (large a_1 in our notation), our model also agrees with the Weber disk and BP results, as long as the height and radius of the cylinder are kept on the same order (see Fig. 3).

Berg and Purcell [3] showed that 3D capture by itself can be remarkably efficient on a sphere, even when the targets occupy only a small fraction of a spherical surface area. Furthermore, 2D diffusion can increase F_{tot} significantly only when the actual rate of capture by 3D is much less than

the maximum possible rate of 3D capture F_{max} as calculated by assuming that the entire surface is a sink. To check this effect in our model, the 3D flux was calculated for cases in which only 3D diffusion exists; i.e., when the surface outside the target is perfectly reflecting. Figure 4 shows the results of this calculation. The fraction F_0/F_{max} (the "3D capture efficiency", defined by eqs. 11 and 13) monotonically decreases from unit as R_2 increases and reaches 0.5 at some value of $a_1 \equiv R_2/R_1$ which depends on the relative height parameter a_2. In qualitative agreement with Berg and Purcell, if the targets occupy as low as 1% of the total surface area (in the case of $a_2 = 100$), the 3D capture efficiency will still be well over 50%. In real biological systems, specific cell surface targets may occupy even far less of the surface area than 1%. Figure 4 also shows that pure 3D capture becomes more efficient as the relative height of the bulk solution a_2 increases. This also corresponds to the Berg and Purcell spherical geometry result that 3D capture becomes more efficient as the radius of the sphere increases relative to the target size R_1. Unless otherwise indicated, we use $a_1 \equiv R_2/R_1 = 100$ and $a_2 \equiv H/R_1 = 100$ in this paper. With that geometry, the 3D capture efficiency is much less than unity and therefore 2D surface diffusion has a chance to enhance F_{tot}.

Figures 5(a–d) explore how the rates of capture per target vary with the surface concentration of targets, for a particular set of diffusion coefficients, kinetic rate constants and target size. These fluxes are plotted as functions of a_1 (the normalized intertarget spacing) for a set of a_2 (normalized cylinder height) values. These results show that both the 3D and the 2D rates of capture per target increase to a limiting value as the intertarget spacing increases. This behavior is expected: as the surface target concentration becomes less, competition between targets is reduced. Figure 5(d) shows that increasing intertar-

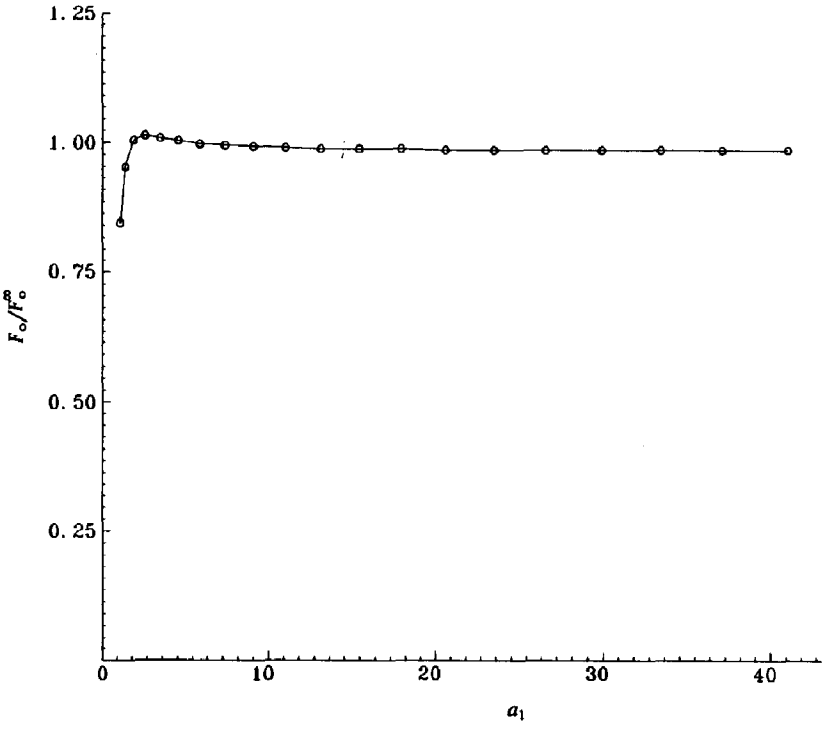

Fig. 3. The effect of geometry on the 3D flux F_0 (assuming reflecting surface outside the receptor, equivalent to setting $D_s = 0$), normalized with respect to F_0^∞, the corresponding 3D flux except with the R_2 and H boundaries set at infinity (Weber's disk). Parameters used: $a_1 = a_2$, $a_3 = 0$, and $a_4 = 0$. After $a_1 = 40$, F_0/F_0^∞ is essentially unity.

get spacing increases the 2D fraction of the total rate of capture. Evidently, 2D capture rates suffer more from target crowding than do 3D capture rates. As cylinder height a_2 increases, both F_{2D} and F_{3D} (therefore F_{tot}) decrease, but the 2D fraction f_{2D} does not seem to vary strongly with the height of the cylinder.

4.2 Dependence on surface diffusion and kinetic rate parameters

The effect of surface diffusion on the rates of capture is demonstrated in Figs. 6(a–d). Each rate is normalized to a constant value for F_0, which is the rate of capture where $D_s = 0$ so that reversible 2D adsorption has no effect on the capture rates. The abscissa in Fig. 6, log a_4^{-1}, increases linearly with log D_s. Increasing D_s increases F_{2D}, F_{tot} and f_{2D} as expected, but decreases F_{3D}. This is because the very success of 2D capture depletes the surface concentration around the target and, through reversible exchange, thereby depletes the local bulk concentration as well. The depletion of bulk concentration then decreases the 3D rate of capture. This effect is magnified as a_3 (proportional to the surface adsorption kinetic rate constant) increases. A larger surface adsorption rate replenishes the surface more quickly and therefore enhances the 2D capture rate. But at the same time, it depletes the bulk more severely so that 3D rate of capture decreases even farther.

Figs. 7(a–d) explore how F_{2D}, F_{3D}, F_{tot}, and f_{2D} vary with the kinetic rate constants for a particular geometry. These capture rates are plotted as functions of a_3 (normalized adsorption rate) for a set of a_4 (normalized desorption rate) values. F_{2D}, F_{tot} and f_{2D} all increase as a_3 increases, but F_{3D} decreases due to the depletion of the bulk concentration by the surface. The larger the normalized desorption rate a_4, the larger must be the normalized adsorption rate a_3 for these effects to occur.

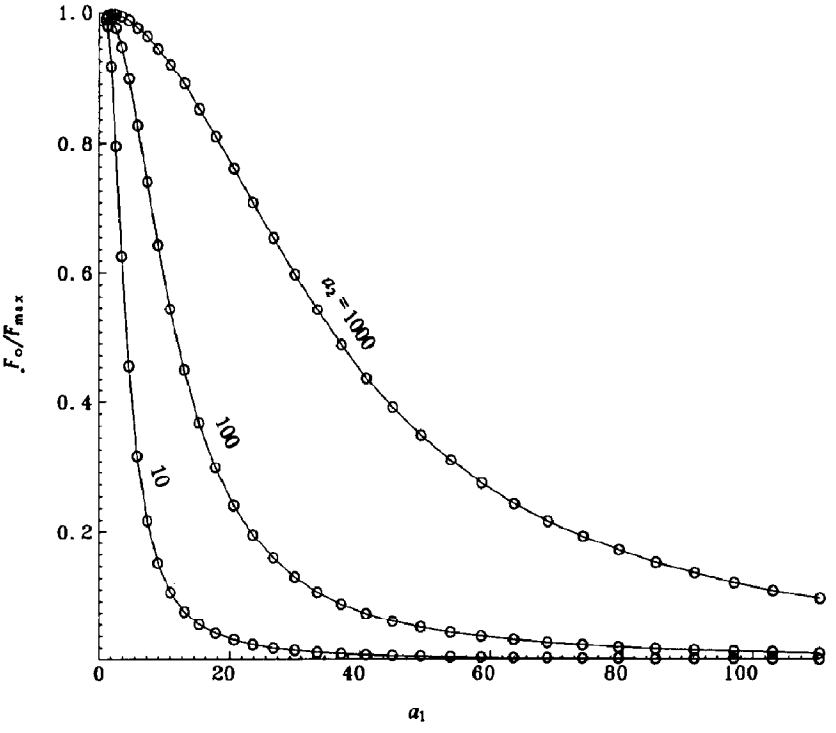

Fig. 4. The effect of surface receptor concentration on the 3D flux for three different relative heights a_2. Parameters used: $a_2 = 10$, 100, or 1000; and $a_3 = a_4 = 0$.

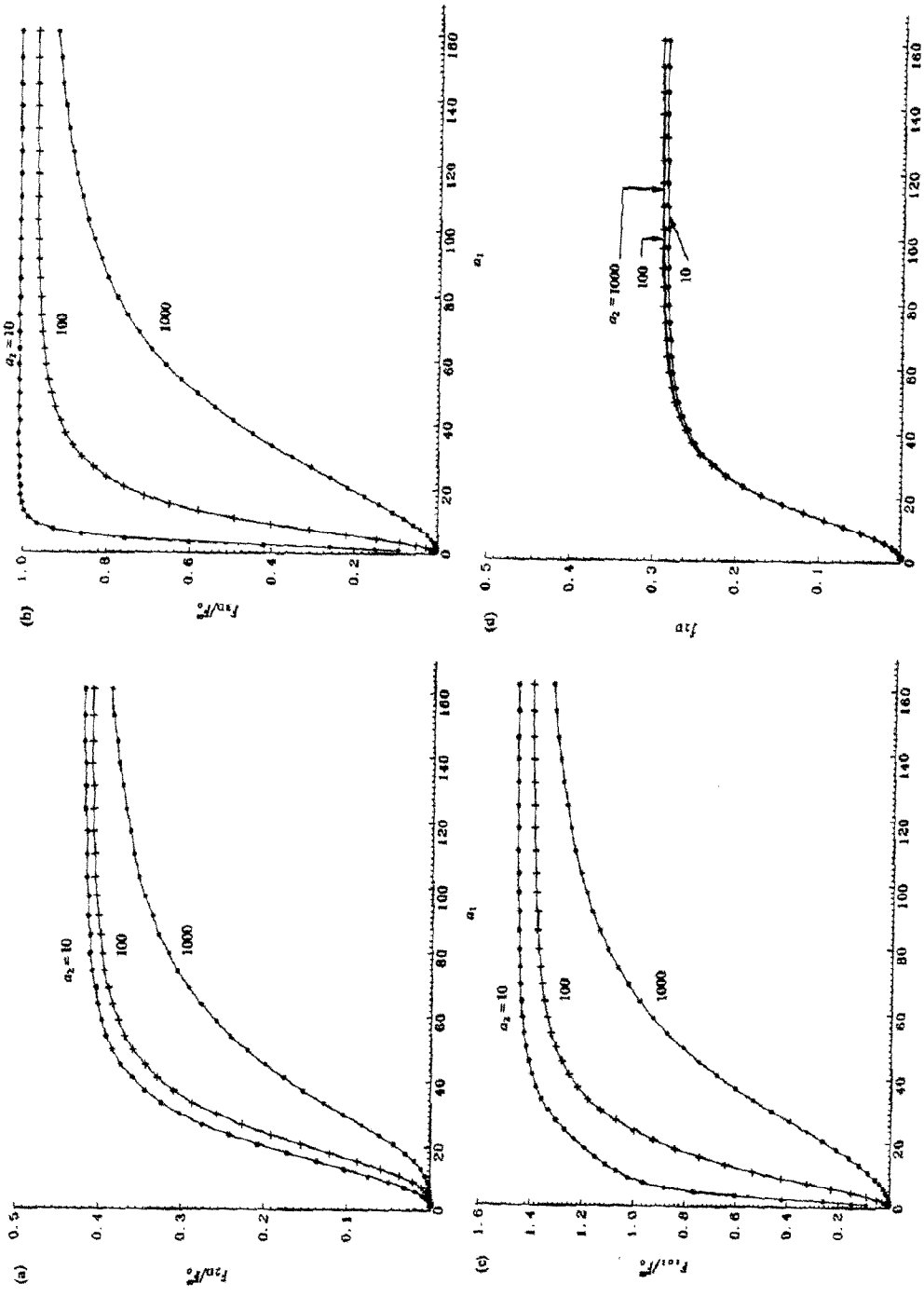

Fig. 5. Dependence upon geometry of (a) F_{2D}; (b) F_{3D}; (c) F_{tot}; and (d) f_{2D}. Parameters used: $a_3 = a_4 = 10^{-3}$.

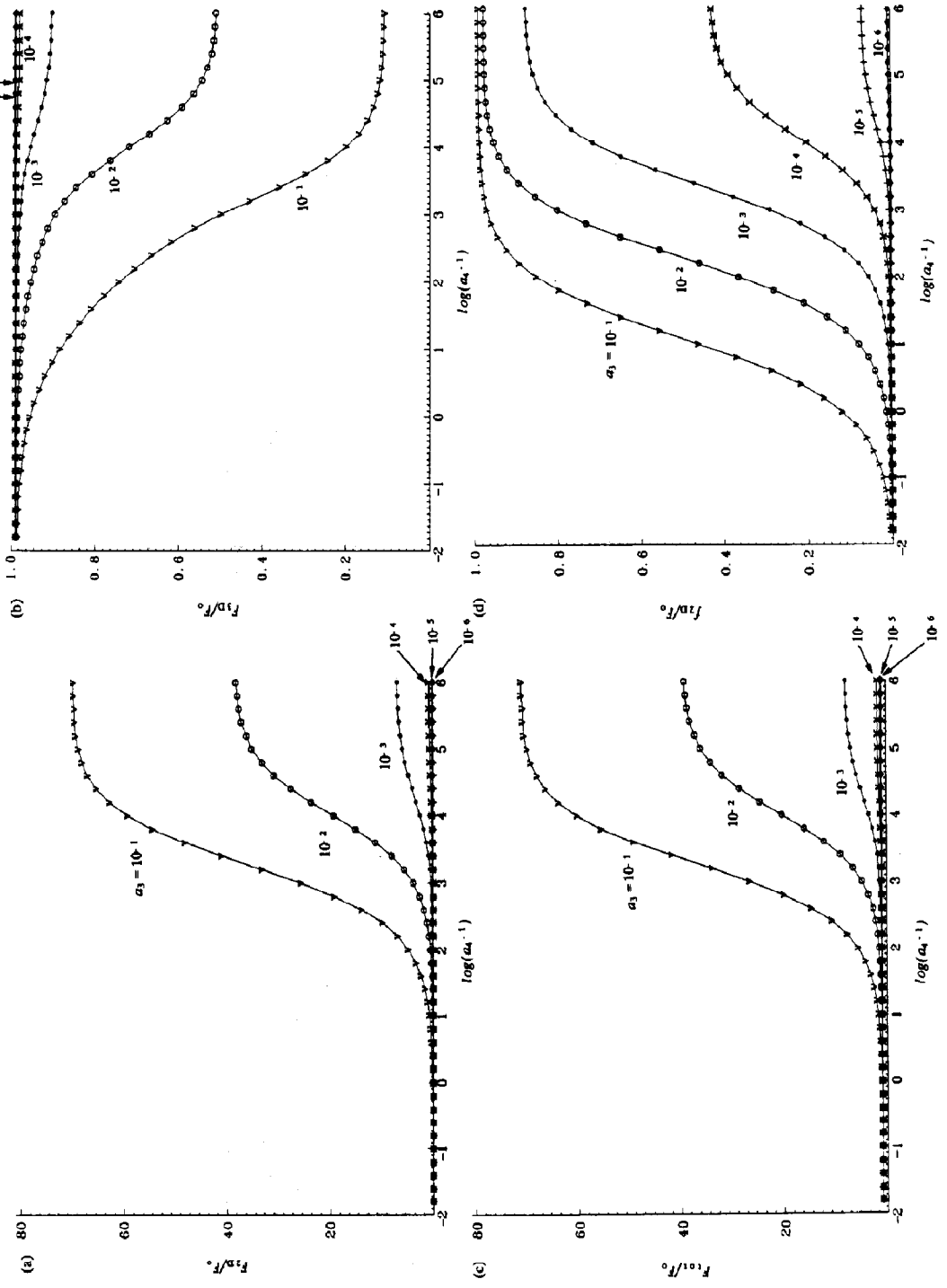

Fig. 6. Dependence upon a_4^{-1} of (a) F_{2D}; (b) F_{3D}; (c) F_{tot}; and (d) f_{2D}. Parameters used: $a_1 = a_2 = 100$, and $F_0 = 3.96DR_1C_0$.

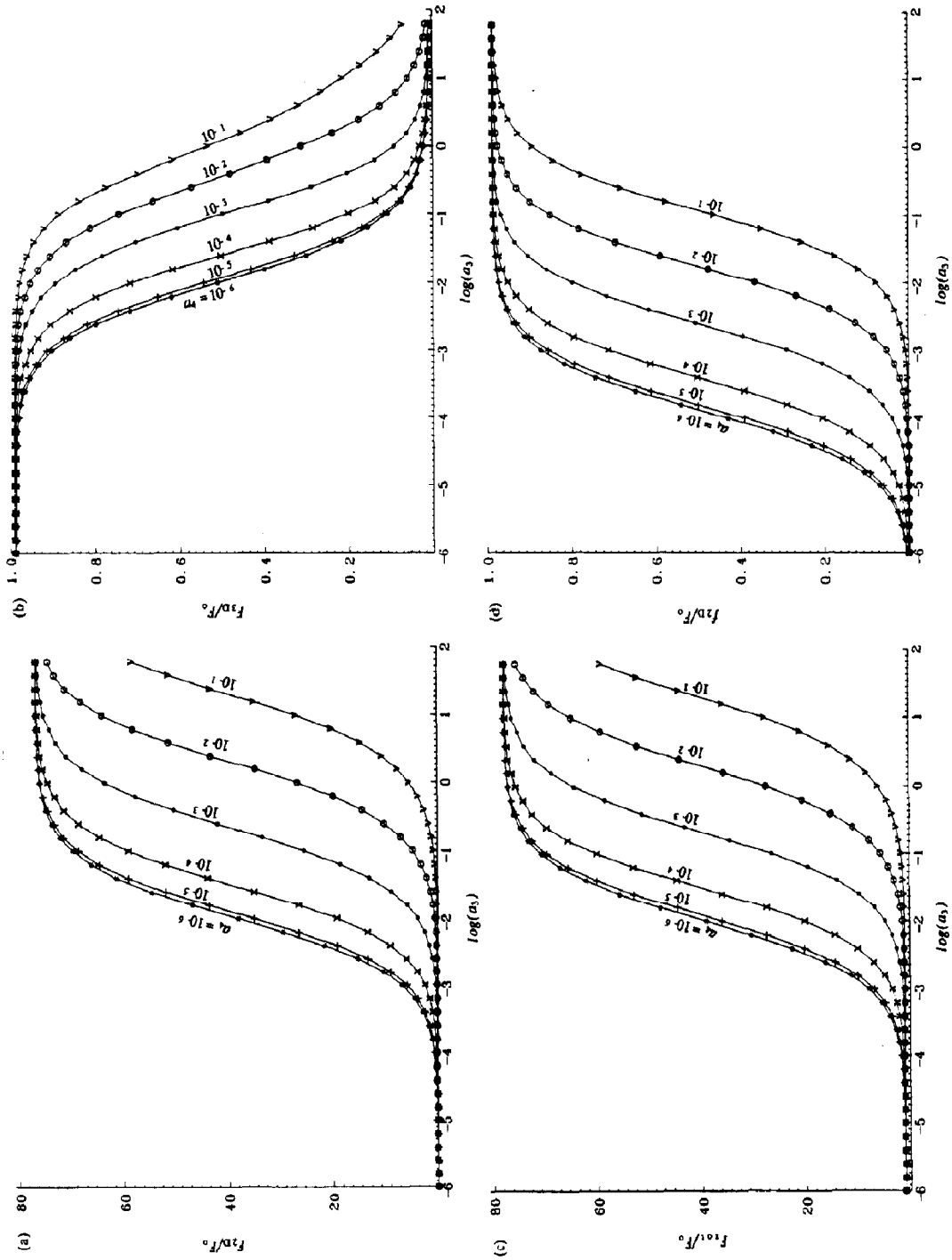

Fig. 7. Dependence upon a_3 of (a) f_{2D}; (b) F_{3D}; (c) F_{tot}; and (d) f_{2D}. Parameters used: $a_1 = a_2 = 100$, and $F_0 = 3.96DR_1C_0$.

4.3 Comparison with earlier models

The results for F_{2D} and F_{3D} in our model differ from those of Berg and Purcell [3] (eqs. 33 and 34) in several respects. For the BP model, eq. (33) states that if F_{2D} and F_{3D} are $\ll F_{max}$, then: (1) F_{2D} is proportional to K_{eq}, i.e., it does not directly depend on k_a and k_d separately but only on their ratio; (2) F_{2D} is proportional to D_s; (3) F_{2D} does not depend on D; and (4) F_{2D} decreases as R_2 increases (as surface target density decreases).

To compare the BP results with our more general results as depicted in Figs. 5, 6 and 7, we must identify where F_{2D} and F_{3D} are much smaller than F_{max}. For the same set of dynamic parameters, these assumptions require a low surface target concentration, i.e., a large a_1 in Figs. 5(a) and (b). For Figs. 6 and 7, note that our $F_0/F_{max} = 0.0125$, so that the assumption of $F_{3D} \ll F_{max}$ is valid throughout Figs. 6(b) and 7(b). The assumption of $F_{2D} \ll F_{max}$ corresponds to the left portion of each curve in Figs. 6(a) and 7(a). At regions where these two assumptions are both valid, none of the above four conclusions flowing from the BP model is consistent with our results:

(1) F_{2D} in Fig. 7(a) does increases as a_3 increases, but is not linearly proportional to a_3 for a constant a_4. Therefore, F_{2D} is clearly not linearly proportional to K_{eq}.
(2) As shown in Fig. 6(a), F_{2D} increases with increasing a_4^{-1} non-linearly. Since $a_4^{-1} \propto D_s$, F_{2D} therefore increases with D_s non-linearly.
(3) Because F_{2D}/F_0 depends non-linearly on a_3 as seen in Fig. 7(a) and $a_3 \propto D^{-1}$, F_{2D}/F_0 is a non-linear function of D^{-1}. However, since F_0 must be linearly proportional to D, then F_{2D} is not independent of D.
(4) As shown in Fig. 5(a), F_{2D} increases with a_1, and thus increases with R_2. This shows that as surface target density decreases, F_{2D} increases and reaches an asymptote.

Our results show that F_{2D} not only depends on K_{eq} non-linearly but also varies with k_d (and therefore also k_a) at any constant K_{eq}. Figures 8(a–d) investigate the dependence of F_{2D}, F_{3D}, F_{tot}, and f_{2D} upon k_d for the same K_{eq}, for a set of various D_s values. Other parameters, such as R_1, R_2, H, D and C_0, are kept constant for these calculations. The region of k_d plotted in these figures satisfies the condition that F_{2D} and F_{3D} are much smaller than F_{max} so that the results can be compared with the BP model. Figure 8 shows that F_{2D}, F_{tot}, and f_{2D} all increase as k_d increases, and the increase is more dramatic as D_s increases. On the other hand, F_{3D} tends to decrease with increasing k_d, and increasing D_s enhances the decrease.

The physical origin of the dependence of the rates of capture on the kinetic rate constants and not just the equilibrium constant can be understood by considering the depletion zones both in the bulk and on the surface. Figures 9(a) and (b) depict these deletion zones for the two different sets of kinetic rate constants: k_a and k_d fast, and k_a and k_d slow, but for the same equilibrium constant K_{eq} and the same surface diffusion coefficient D_s. Faster kinetic rates replenish the surface adsorbed ligand more quickly and increase the 2D rate of capture while diminishing the width of the surface depletion zone. However, faster replenishment of the surface also depletes the bulk ligand more rapidly so that the bulk has a larger depletion zone. The net effect then is to increase F_{2D}, F_{tot}, and f_{2D}, but to decrease F_{3D}.

Figures 10(a) and (b) depict the depletion zones for two different surface diffusion coefficients but the same set of kinetic rate constants. Increasing D_s increases the 2D rate of capture and gives rise to a wider depletion zone on the surface as more distant adsorbed ligands are likely to encounter the target. But this wider surface depletion zone depletes the bulk ligand more rapidly, and thereby causes the bulk to have a larger depletion zone as well. The 3D capture rate thereby decreases.

Our results also can be compared with those of OB model by plotting the results for F_{tot}/F_0^{∞} (Fig. 11a) and f_{2D} (Fig. 11b) vs. a_3/a_4 (the normalized adsorption/desorption equilibrium constant) from both models. A large boundary is chosen in order to simulate the infinity boundary in the OB model. A corresponding pair of graphs (Figs. 12a and b) displays the same range of equilibrium constants but faster kinetic rates. Comparison of

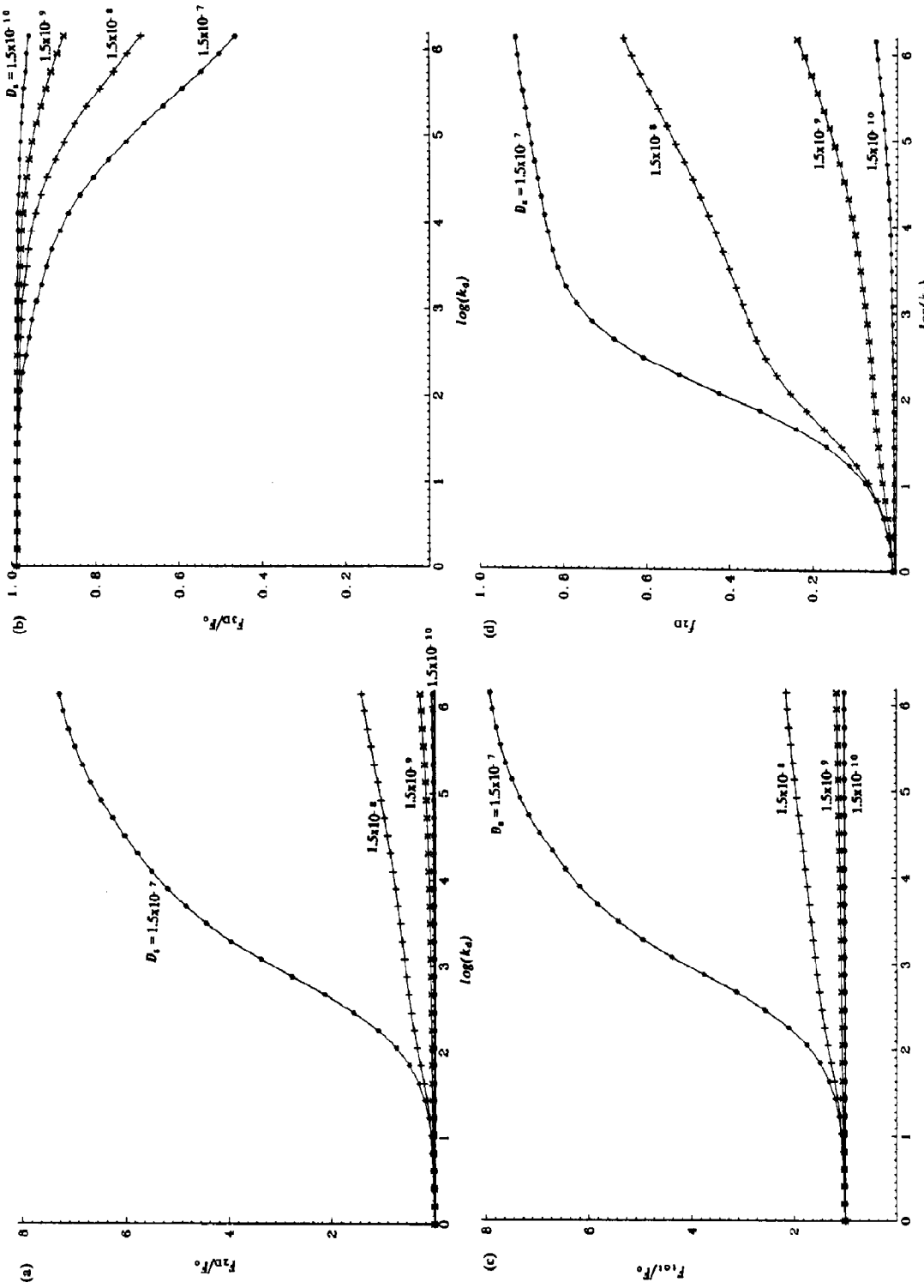

Fig. 8. Dependence upon k_d of (a) F_{2D}; (b) F_{3D}; (c) F_{tot}; and (d) f_{2D}. Parameters used: $a_1 = a_2 = 100$, $D = 1.5 \times 10^{-6}$, $K_{eq} = 1.5 \times 10^{-5}$, $R_1 = 0.1$, and $F_0 = 3.96 DR_1C_0$.

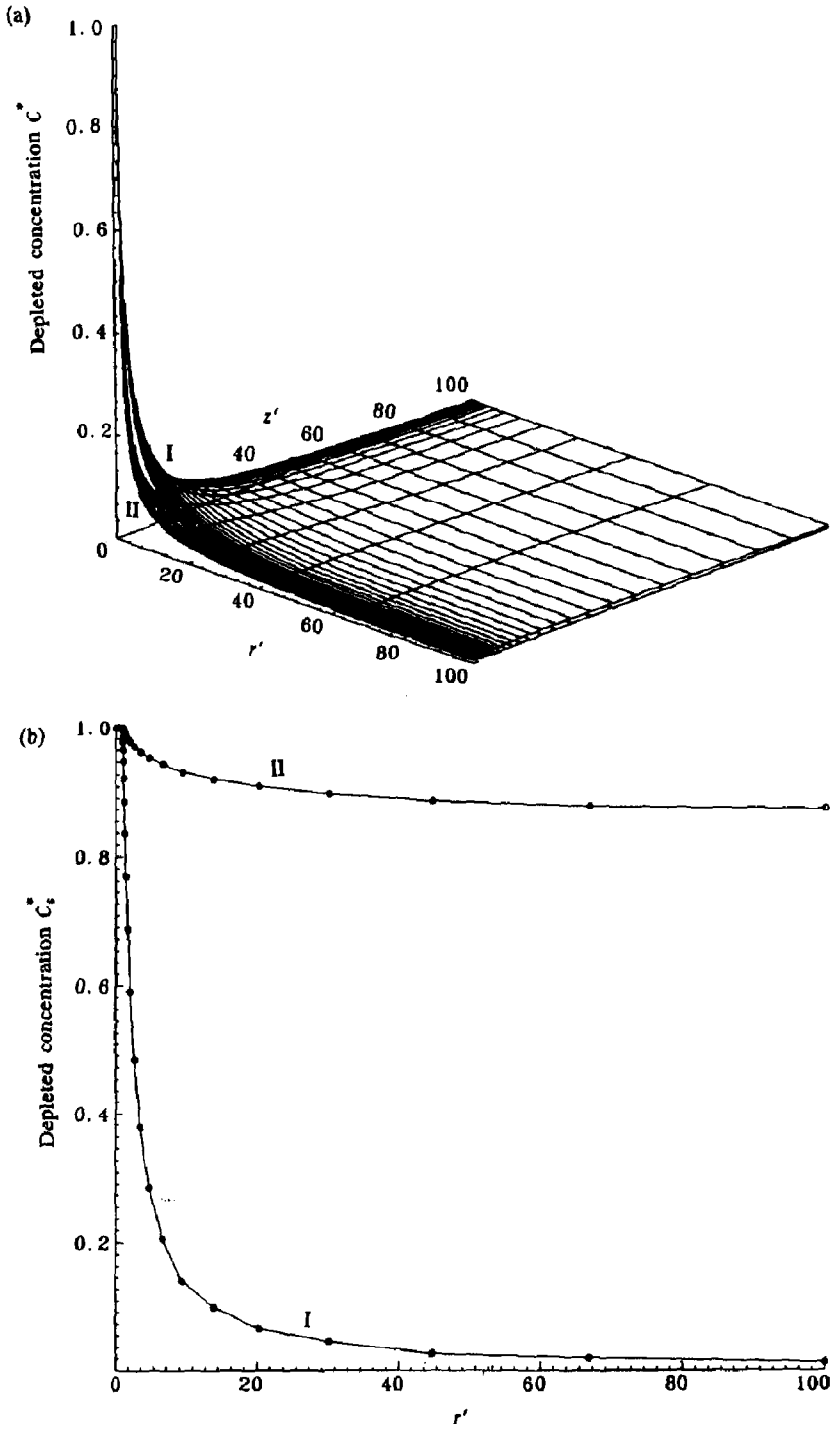

Fig. 9. (a) Effect of kinetic rate constants on bulk depletion zones. The ordinate axis is the depleted concentration defined as $C^* = 1 - C/C_0$. (b) Effect of kinetic rate constants on surface depletion zones. The ordinate axis is the depleted concentration defined as $C_s^* = 1 - C_s/C_0K_{eq}$. Parameters used: $a_1 = a_2 = 100$, $D = 1.5\times10^{-6}$, $K_{eq} = 1.5\times10^{-5}$, $D_s = 1.58\times10^{-8}$, $R_1 = 10^{-7}$. Curve I: $k_d = 10^6$, and curve II: $k_d = 10$.

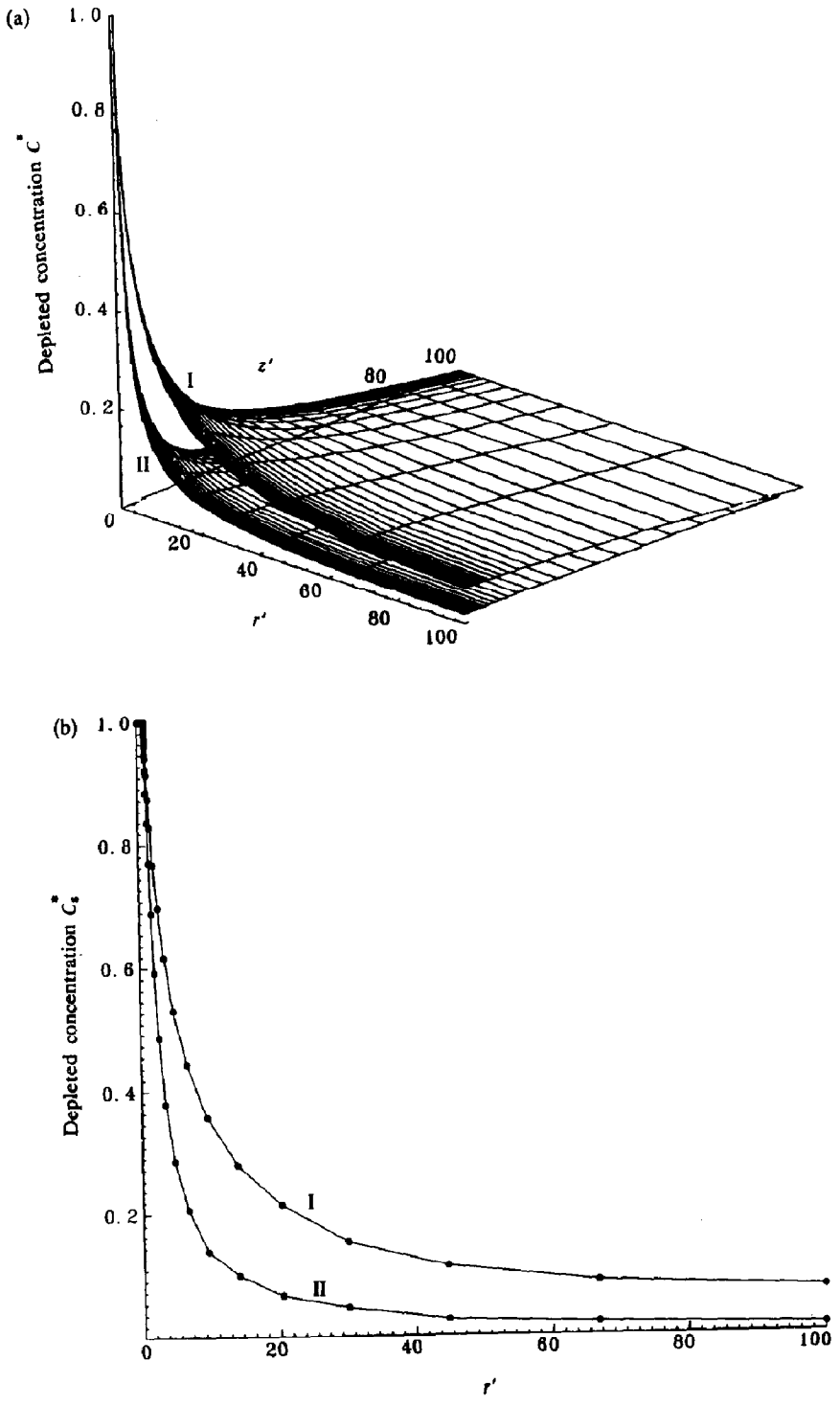

Fig. 10. Effect of surface diffusion on (a) bulk depletion zones, and (b) surface depletion zones. C^* and C_s^* ordinates are defined as in Fig. 9. Parameters used: $a_1 = a_2 = 100$, $D = 1.5\times10^{-6}$, $K_{eq} = 1.5\times10^{-5}$, $k_d = 10^6$, $R_t = 10^{-7}$. Curve I: $D_s = 1.5\times10^{-7}$, and curve II: $D_s = 1.5\times10^{-8}$.

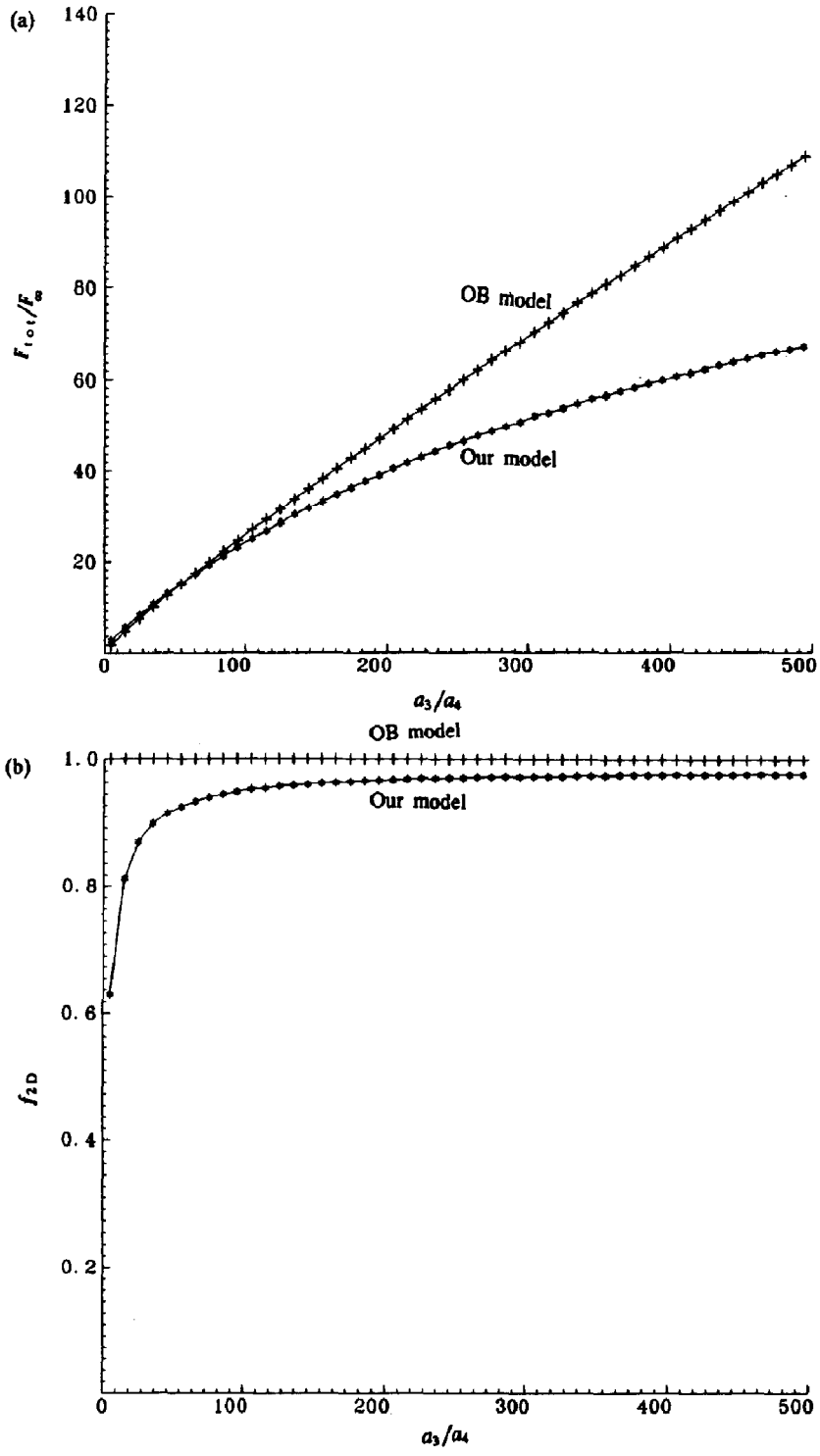

Fig. 11. A comparison of the present model with the Otto Berg (OB) model at slow kinetic rates as a function of a_3/a_4: (a) F_{tot}, and (b) f_{2D}. Parameters used: $a_3 = 10^{-3}$, and $a_1 = a_2 = 500$.

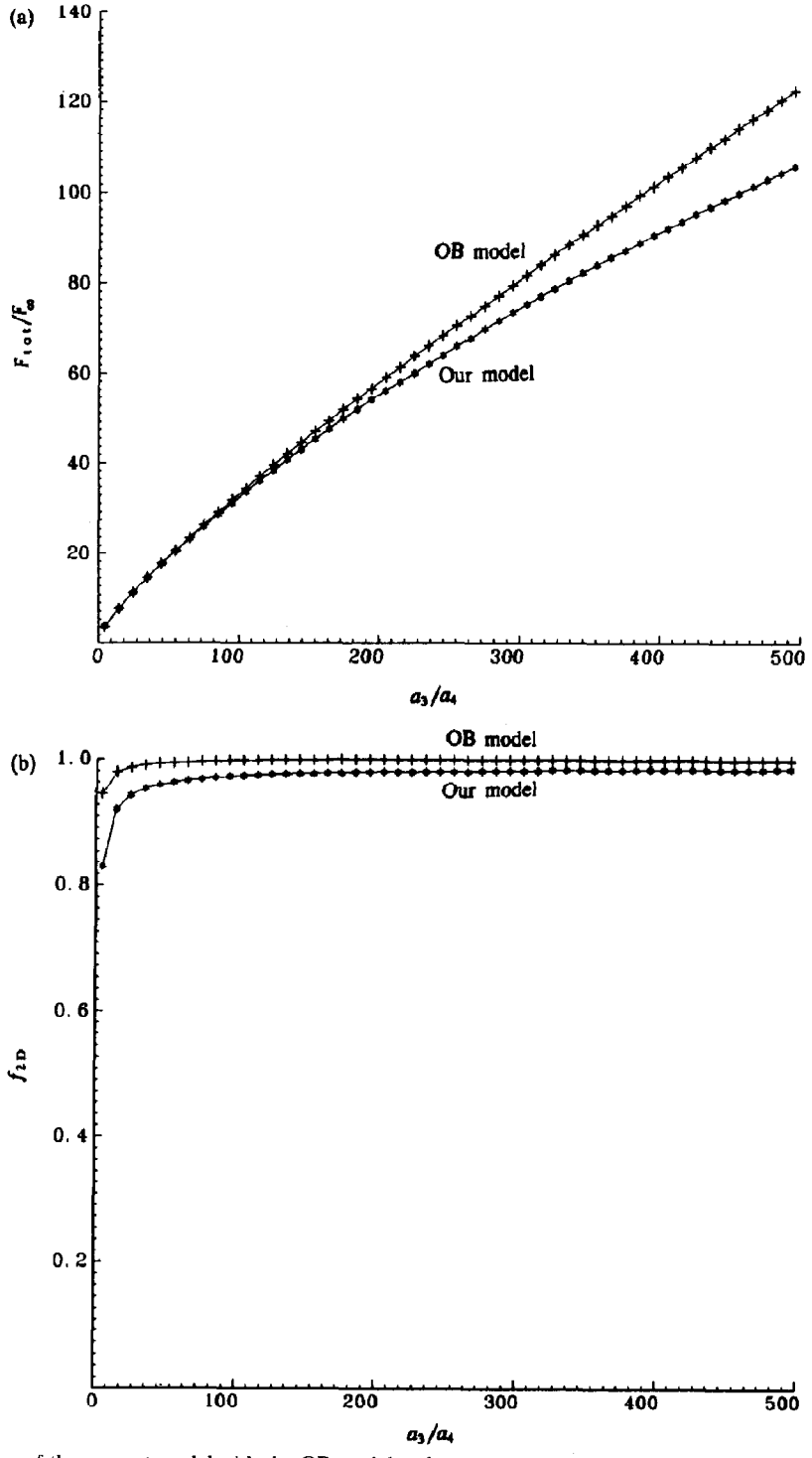

Fig. 12. A comparison of the present model with the OB model at fast kinetic rates as a function of a_3/a_4: (a) F_{tot}, and (b) f_{2D}. Parameters used: $a_3 = 1$, and $a_1 = a_2 = 500$.

Figs. 11 and 12 show that the two models approach each other as the kinetic rates become faster. This is not surprising since the OB model is more appropriate for the limiting case of a_3 and $a_4 \to \infty$, whereas our model does not have this constraint.

5. Discussion and conclusions

Ligands can be captured by a surface target either through direct bulk diffusion or surface diffusion following reversible adsorption to the surface. Given the presence of nonspecific adsorption, the ability of the adsorbed ligands to surface diffuse will always enhance reaction rates with a perfect sink target located in the surface in steady state. The questions addressed here are: (a) under what conditions does the enhancement become significant; and (b) how does the magnitude of the enhancement depend on the physical parameters?

Correct prediction of the relative contribution of the 2D and 3D pathways to the total rate of capture can help to elucidate the mechanism by which the target captures ligands. We have solved a steady state boundary value problem for a perfect sink disk target in the surface, taking into account bulk and surface diffusion coefficients D and D_s and adsorption/desorption kinetic rate constants k_a and k_d at non-target regions. Solutions have been successfully found by numerical computation on a PC. The results show that the rate of capture from the surface depends non-linearly on D_s, K_{eq}, k_a, k_d and geometrical dimensions. In particular, we demonstrate that not only is the non-target reqion equilibrium constant K_{eq} important in determining the rate of capture from the surface, but so are the kinetic rate constants k_a and k_d separately. As is clear from Fig. 8, the dependence on the kinetic rate constants individually is quite strong for all situation in which the 2D flux is significant; in the ranges shown, there is no limit beyond which these kinetic rate constants individually are not important.

In all cases, the combination of surface adsorption and diffusion enhances the total rate of capture. The results should be useful for predicting 3D and 2D reaction rates of biological membrane bound receptor clusters and substrate-immobilized enzymes. The rate parameters that are needed for this prediction, the kinetic rate constants and surface diffusion coefficient, are all calculatable from measurements taken with available experimental techniques, notably by total internal reflection/fluorescence recovery after photobleaching [10–13].

The geometries usually chosen for simplicity in diffusional capture calculations—isolated or uniformly spaced sinks on a sphere with a ligand source at infinity or, as presented here, uniformly spaced targets on a plane with a ligand source at a finite distance H above the plane—are clearly not "general". The particular geometrical assumptions do affect the absolute rates of capture. However, the most significant results in our calculations, the relative rates of 2D vs. 3D capture given by f_{2D}, are rather insensitive to changes in the intertarget distance $2R_2$ and the ligand source height H over a large range (e.g., for $a_1 = R_2/R_1$ greater than 40 and for $a_2 = H/R_1$ greater than 10 with the particular other parameters as chosen for Fig. 5d). Therefore, we would expect our approach for calculating f_{2D} to be valid even if the sinks were spaced randomly (but sparsely) rather than uniformly, and if the surface were curved rather than flat. We would expect the approach to be less valid for randomly (but densely) distributed receptors where the average spacing between sinks is small, which for our parameters means $R_2/R_1 < 40$. Nevertheless, the approach is completely unrestricted with respect to choice of H; the figures assume $H \gg R_1$ only for easier comparison with previous models.

The absolute rates are a more sensitive function of geometry than the relative rates. This is a general difficulty with calculations modeling chemoreception: an actual biological receptive surface is nowhere close to being either an isolated sphere in a ligand sea of infinite depth nor a plane in a finite sea. The calculations described here, which offer a_1 and a_2 as input parameters, show both the effects of varying the cylinder height and radius (e.g., Figs. 3 and 5) and the approximate range of geometrical parameters over which the exact geometry is not critical.

The treatment here is "exact" in the sense that no limiting approximations were employed to solve the assumed model, and the results should be valid over a wide range of rate constants, surface target densities, and diffusion coefficients. However, the assumption that the target is a perfect sink is not necessarily appropriate for all cases of specific binding to a surface target. Presumably, if the sink is irreversible but "imperfect" in that not every collision leads to disappearance of the ligand, then the target still can be modeled as perfect sink but with a smaller radius. On the other hand, if binding to the target is reversible so that the ligand eventually returns unaltered to the surroundings (as does acetylcholine at its receptor), then the steady state solution describes an equilibrium situation with no net flows. In that case, no depletion zone exists in steady state and the theory contained herein is inappropriate. "Collision" rather than "capture" rates become relevant, and it is still likely that 2D diffusion significantly enhances the total rate of collision. However, since the ligands and receptors are in reversible equilibrium, the non-specific kinetic rate constants k_a and k_d will affect the degree of enhancement only through their ratio, the equilibrium constant K_{eq}.

Although a biological cell surface receptor is often modeled in the literature as a perfect sink, it may capture just one ligand and then the whole complex effectively disappears via internalization, migration to coated pits, etc, to be replaced on the average by another receptor at a random location. Of course, statistical local depletion zones of tiny amplitude do develop around the bound-up receptors, but the newly incorporated receptors appear elsewhere in general and, on the average, they do not sample those local depletion zones. Therefore, all new binding occurs in a statistically uniform concentration, and the theory herein is again inappropriate. However, a non-local 3D depletion zone may still develop over the whole surface, which acts as an imperfect but irreversible sink. The profile and depth of this nonlocal depletion zone, and the 2D diffusion enhancement of the overall rate of irreversible capture by the surface, may still be functions of k_a and k_d separately (not just through K_{eq}). The details of a solution to this problem remain to be worked out.

Acknowledgements

Special thanks to Dr. Robert M. Fulbright for his generous help and important suggestions on the theory and the programming. We also thank Dr. M.J. Weinstein for his helpful advice in trying to solve the problem analytically, Dr. P.L. Roe for his help in searching for numerical methods, and Dr. Nancy L. Thompson for many useful discussions on this topic. This project was supported by NIH 14565 and NSF DMB-8805296 to D.A.

References

1 G. Adam and M. Delbrück, in: Structural chemistry and molecular biology, eds. A. Rich and N. Davison (W.H. Freeman, San Francisco, CA, 1968) p. 198.
2 D. Axelrod, J. Membrane Biol. 75 (1983) 1.
3 H. Berg and E. Purcell, Biophys. J. 30 (1977) 193.
4 O. Berg, Biophys. J. 47 (1985) 1.
5 R.I. Cukier, J. Chem. Phys. 79 (1983) 2430.
6 A. Rosevear, J.F. Kennedy, and J.M.S. Cabral, Immobilized enzymes and cells (Hilger, Philadelphia, PA, 1987).
7 G. Venkatakrishnan, C.A. McKinnon, C.G. Pilapil, D.E. Wolf and A.H. Ross, Biochemistry 30 (1991) 2748.
8 M.A. McCloskey and M.-M. Poo, J. Cell Biol. 102 (1986) 88.
9 R. Schranner and P.H. Richter, Biophys. Chem. 8 (1978) 135.
10 N. Thompson, T. Burghardt, and D. Axelrod, Biophys. J. 33 (1981) 435.
11 D. Axelrod, E.H. Hellen and R.M. Fulbright, in: Topics in fluorescence spectroscopy, Vol. 3: Biochemical applications, ed. J. Lakowicz (Plenum, New York, NY, 1992), p. 289.
12 E.H. Hellen and D. Axelrod, J. Fluorescence 1 (1991) 113.
13 R.M. Fulbright and D. Axelrod, submitted.
14 J. Crank, The mathematics of diffusion, second edition (Oxford, New York, 1975) p. 42.
15 W.H. Press, B.P. Flannerry, S.A. Teukolsky, and W.T. Vetterling, Numerical recipes (Cambridge, New York, NY, 1989) Chap. 17.
16 D.A. Anderson, J.C. Tannehill, and R.H. Pletcher, Computational fluid mechanics and heat transfer (Hemisphere, New York, NY, 1984) p. 247.